Feasibility of Low-Cost Infrared Thermal Imaging to Assess Occupants' Thermal Comfort

Da Li[1]; Carol C. Menassa, Ph.D.[2]; and Vineet R. Kamat, Ph.D.[3]

[1]Ph.D. Candidate, Dept. of Civil and Environmental Engineering, Univ. of Michigan, Ann Arbor, MI 48109. E-mail: dliseren@umich.edu
[2]Dept. of Civil and Environmental Engineering, Univ. of Michigan, Ann Arbor, MI 48109. E-mail: menassa@umich.edu
[3]Dept. of Civil and Environmental Engineering, Univ. of Michigan, Ann Arbor, MI 48109. E-mail: vkamat@umich.edu

ABSTRACT

Understanding occupants' thermal comfort is essential for the effective operation of heating, ventilation, and air conditioning (HVAC) systems. Existing studies of the "human-in-the-loop" HVAC control generally suffer from: (1) excessive reliance on cumbersome human feedback; and (2) intrusiveness caused by conventional data collection methods. To address these limitations, this paper investigates the low-cost thermal camera as a non-intrusive approach to assess thermal comfort in real time using facial skin temperature. The framework developed can automatically detect occupants, extract facial regions, measure skin temperature, and interpret thermal comfort with minimal interruption or participation of occupants. The framework is validated using the facial skin temperature collected from twelve occupants. Personal comfort models trained from different machine learning algorithms are compared and results show that random forest model can achieve an accuracy of 85% and also suggest that the skin temperature of ears, nose, and cheeks are most indicative of thermal comfort.

INTRODUCTION AND BACKGROUND

Lack of thermal comfort in buildings is a common problem where studies reveal that up to 43% of building occupants are dissatisfied with the indoor thermal environment, which can lead to sick building syndrome, health complications, and reduced productivity (Karmann et al. 2018). On the other hand, HVAC systems represent the largest energy end-use accounting for more than 50% of the total energy required to operate residential and commercial buildings (DOE 2017). Therefore, there will be significant social and economic benefits if building HVAC systems can be optimized to improve occupants' comfort, satisfaction, and health while achieving reduced energy consumption (Li et al. 2017a, 2017b). To this end, researchers need to understand occupants' thermal preferences and needs in real time.

To address this research question, existing studies have extensively investigated the "human-in-the-loop" approach which integrates human participation into controlling the HVAC systems or personal heating/cooling devices (Jazizadeh et al. 2013, Kim et al. 2018, Li et al. 2017b, 2017c). This category of studies focuses on developing personal comfort prediction models using occupants' feedback or bio-signal data, which have been suggested to outperform the Predicted Mean Vote (PMV) and adaptive models. For example, Li et al. (2017b) proposed an HVAC control framework which used wristband sensors, smartphone applications, and environment sensors to collect human and environmental data, such as skin temperature, heart rate, clothing level, thermal preference, and room temperature. Personal comfort models developed in this study achieved an 80% accuracy in predicting the three-point thermal preference (i.e., warmer, no change, cooler). Kim et al. (2018) developed a personal comfort chair which can record

heating and cooling requests from occupants under various room conditions. This study compared the predictive performance of different machine learning algorithms and reported a 73% accuracy in thermal preference prediction.

Despite the significant contributions of the aforementioned studies in assessing occupants' thermal comfort, these approaches are intrusive and can cause interruption of building occupants. First, this human participation oriented solution relies on occupants' continuous feedback to interpret their comfort states over time. This is based on the assumption that the human body is the best "comfort sensor" which can periodically indicate the need to adjust the indoor thermal condition through feedback (e.g., requests to make the room warmer or cooler). However, in practice the frequency of feedback tends to decrease with time as the novelty and excitement of the system fades away (Li et al. 2017b). In addition, the requirement of human input is distracting during regular work time, especially over heavy workload periods. Moreover, these studies require occupants to use wearables (e.g., wrist-worn sensors), certain devices (e.g., comfort chair) or mobile applications, which is inconvenient and also lacks scalability.

On the other hand, it is well established that thermal conditions can affect human thermoregulation (e.g., vasodilation and vasoconstriction) (Charkoudian 2003), which can lead to changes in the skin temperature. Therefore, to address the limitation of intrusiveness in existing studies, infrared thermal imaging is an ideal tool as it can collect an individual's skin temperature and interpret the thermal comfort without direct contact with the skin surface. Specifically, human face is selected as the region of interest as (1) faces have a higher density of blood vessels than other locations, which can lead to more significant variations in skin temperature when ambient thermal environment changes; and (2) faces are usually not covered by clothing and thus the emitted infrared energy can be directly measured by thermal cameras.

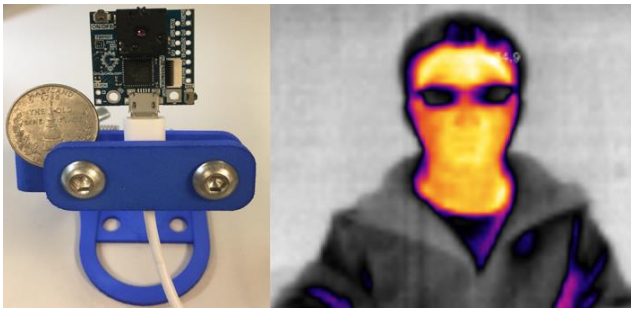

Figure 1. Lepton (left) and the facial thermal imaging (right)

Table 1. Specifications of Lepton

Features	Descriptions
Dimensions	8.5 x 11.7 x 5.6 mm
Resolution	80(h) x 60(v) pixels
Thermal sensitivity	< 50 mK
Accuracy	±5 ˚C or ±5% of reading
Price	$ 199

OBJECTIVES

This paper explores the feasibility of low-cost infrared thermal imaging as a truly non-intrusive data collection approach to interpret human thermal comfort in indoor environments in real time. To achieve this objective, the authors developed an approach to non-intrusively obtain,

retrieve, and analyze facial skin temperature features for each building occupant in real operational indoor environments using thermal cameras, computer vision, and machine learning techniques. In addition, we extended Li et al. (2018) by comparing different machine learning algorithms in the comfort prediction.

TECHNICAL APPROACH

Low-cost thermal camera

This study used the FLIR Lepton 2.5 radiometric thermal camera (hereinafter referred to as the Lepton) to collect skin temperature data (see Figure 1) (FLIR 2014). Lepton is an uncooled long-wave infrared thermal imaging core with factory-calibrated temperature measurements. The relevant specifications of Lepton can be found in Table 1.

Data collection and analysis

Figure 2 illustrates the workflow of the proposed non-intrusive thermal comfort interpretation framework. This framework leverages a range of techniques including: (1) computer vision to detect human faces; (2) facial geometry to locate different facial regions; (3) signal processing methods to clean the raw skin temperature data; and (4) machine learning algorithms to develop personal comfort models and identify important features. Details of each step are explained in the following subsections.

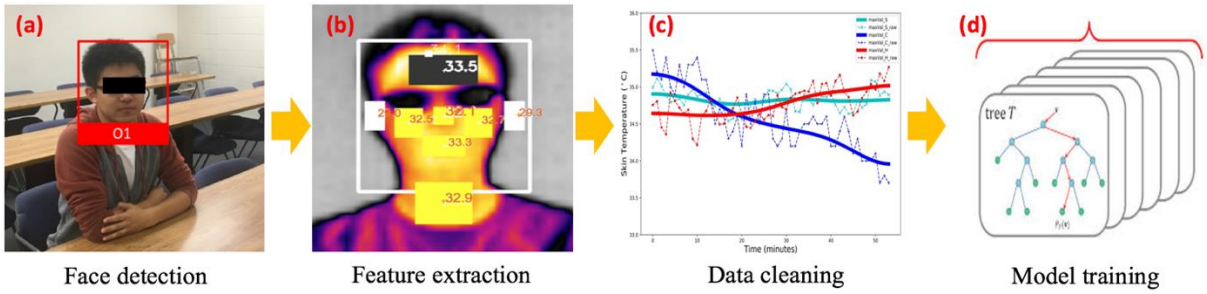

Figure 2. The workflow of the non-intrusive thermal comfort interpretation framework

Face detection

The Haar Cascade algorithm was applied to detect human faces using the OpenCV package (Figure 2a). Haar Cascade is a fast and effective face detection algorithm, which recognizes frontal and profile faces by checking the existence of certain edges or textures in the image (Viola and Jones 2001). Although the Lepton has a low resolution of 80 by 60 pixels, the outlines of facial contours are clearly preserved in the thermal image (see Figure 2b, the image was taken one meter away from the occupant to represent a non-intrusive distance), which makes the Haar Cascade algorithm suitable for this task.

Feature extraction

After detecting human faces, different facial regions were located based on the facial geometry, which include the forehead, nose, cheeks, ears, mouth, and neck (see Figure 2b, each region was highlighted for the demonstration purpose). The area and location of each facial region were tuned on several subjects prior to the data collection experiment to ensure all

features can be detected across different subjects. Then, temperature measurements of each identified region were extracted to produce skin temperature features. In this study, a total of 26 skin temperature features were extracted including (1) global temperature features: the maximum and minimum value of the whole face; and (2) local temperature features: the lowest, highest, mean, and gradient temperature of each facial region. The authors also conducted a preliminary experiment to evaluate the accuracy of the Lepton by comparing its measurements with a reference FLIR T450SC camera. Details about the comparative experiment can be found in Li et al. (2018).

Data cleaning

Two types of measurement errors of skin temperature were considered: (1) measurements of non-facial features, e.g., hands are falsely detected as the mouth region when a subject drinks water during the experiment, which corresponds to a spike in the raw data; and (2) the random measurement error of the thermal camera which can be assumed to follow a Gaussian distribution with a zero mean. In this study, the authors first applied a median filter to remove large spikes in the raw data and averaged image frames captured in every minute. Then, a Gaussian filter was applied to smooth the raw data. Figure 2c shows a subject's skin temperature measurements in the experiment (detailed in section 4) where the thin broken lines represent the raw data from the thermal camera and the thick solid lines represent the processed data after removing outliers and smoothing. It is obvious that large measurement errors have been removed through the data cleaning and the increasing and decreasing trends of skin temperature are well preserved.

Model training

The prediction of thermal preference is a classification problem with three categorical values, i.e., warmer, cooler, and neutral. Thus, the personal model is formulated as $TP = \mathcal{F}\left(T_{facial}, \nabla_{facial}\right)$, where TP is the target variable thermal preference, and T_{facial}, ∇_{facial} are the skin temperature features and the corresponding gradients.

To train personal comfort models for each subject, various machine learning methods can be compared to select the best performing algorithm (Kim et al. 2018). In this study, we compared four widely used algorithms including Random Forest (RF), Classification Tree (CTree), Support Vector Machine (SVM), and Logistic Regression (LR). We used the Python Scikit-learn package to train the model and tuned the hyper-parameters through grid search for performance optimization. For example, the hyper-parameters for the RF model were searched through ['n_estimators': [300, 500, 700, 1000], 'max_features': ['auto', 'sqrt', 'log2']; 'max_depth': [2, 3, 4, 5]. In the RF model, the maximum number of features allowed in each estimator and the maximum tree depth were intentionally controlled at a small size to reduce the problem of overfitting.

EXPERIMENTAL SETUP

The authors conducted an experiment to collect the skin temperature data and subjects' responses in a research office at the University of Michigan (UM) during the heating season from December 2017 to February 2018. The average high and low outdoor temperature was 1.6 °C and -6.7 °C, correspondingly. In the testbed office, a thermal camera was placed one meter away from the subject which monitors the frontal face (see Figure 3). The testbed office had two

COZIR temperature (accuracy: ±1 °C) and humidity sensors (accuracy: ±5%) to continuously collect the ambient data within the close proximity to the subject during the experiment.

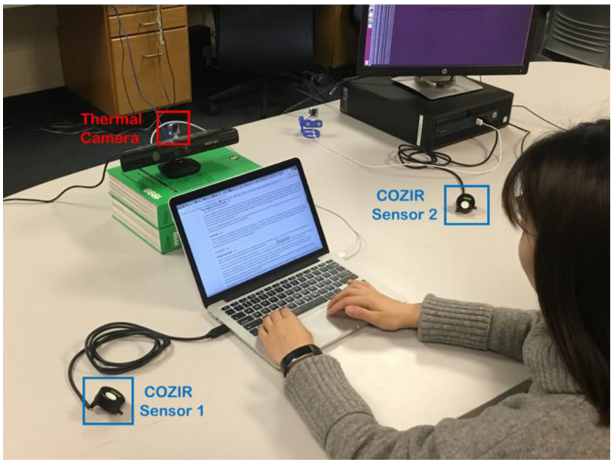

Figure 3. Experimental setup

Twelve subjects participated in the experiment consisting of four phases as outlined in Figure 4. In the preparation phase, subjects were provided with a customized phone app to report their thermal preferences during the experiment through a three-point scale, i.e., warmer, cooler, neutral. Details about the phone app can be found in Li et al. (2017b). In the following 60-min steady-state phase, subjects were asked to perform regular office activities such as reading, typing, or browsing. In this phase, room temperature was maintained at 25 °C to represent a neutral steady-state condition. Next, the heating (room temperature increased from 22 °C to 28 °C) or cooling phase (room temperature decreased from 28 °C to 22 °C) started in a random order. The COZIR sensors showed that in both phases the room temperature approximately changed at a constant rate of ±1 °C per 10 minutes. The random order of heating and cooling experiments was designed to eliminate subjects' bias in thermal sensation and comfort. For example, if a subject knows the current room temperature is decreasing, he or she may unconsciously think it is getting cold. The data collection experiment has been approved by the UM Institutional Review Board (IRB) for conducting human subjects research.

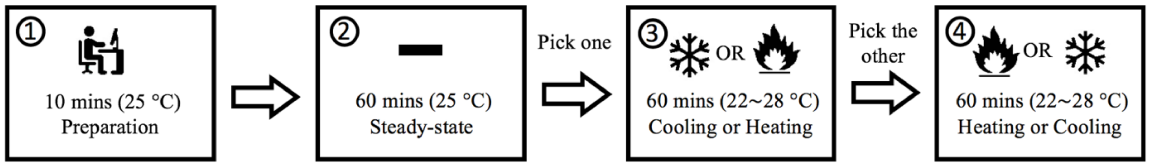

Figure 4. Timeline of the data collection experiment

RESULTS AND DISCUSSION

Appendix Table A.1 presents a summary of the skin temperature statistics in the experiment. The mean and standard deviation (*SD*) of each feature were calculated from the Eq. (1) and Eq. (2) as shown below.

$$\bar{\mu} = \frac{1}{n}\sum_{k=1}^{n}\mu_k,\ SD(\bar{\mu}) = \sqrt{\frac{1}{n-1}\sum_{k=1}^{n}(\mu_k - \bar{\mu})} \quad (1)$$

$$\bar{s} = \frac{1}{n}\sum_{k=1}^{n} s_k,\ SD(\bar{s}) = \sqrt{\frac{1}{n-1}\sum_{k=1}^{n}(s_k - \bar{s})} \quad (2)$$

Where $\bar{\mu}$ and $SD(\bar{\mu})$ are the mean and *SD* of skin temperature of all subjects in a particular phase; $\bar{s}$ and $SD(\bar{s})$ are the mean and *SD* of the sample standard deviation; n is the number of subjects.

As shown in Appendix Table A.1, the variations of skin temperature in the cooling (column 2) and heating (column 4) phases were much larger than those in the steady-state phase (column 6), which implied that skin temperature was affected by the room temperature. Moreover, nose and ears regions had a larger temperature variation compared to other regions in the cooling (nose: 0.60 ± 0.25 °C, ear: 0.67 ± 0.20 °C) and heating phases (nose: 0.77 ± 0.34 °C, ear: 0.71 ± 0.43 °C). Skin temperature features from these two regions are useful to predict thermal preferences as they are sensitive to the change of the environment. For more details please refer to Li et al. (2018).

After tuning the hyper-parameters, ten-fold cross-validations were conducted to evaluate the personal comfort models developed using different algorithms. As shown in Table 2, the RF algorithm achieved the best performance most of the time, which is consistent with the results in Kim et al. (2018). On average, by using the selected facial skin temperature features, personal comfort models can achieve an 85.0% accuracy in predicting subjects' thermal comfort preferences.

Table 2. Prediction accuracy of different algorithms for each subject

ID	1	2	3	4	5	6	7	8	9	10	11	12	Avg.
SVM	0.71	0.72	0.81	0.88	0.74	0.73	0.83	0.75	0.66	0.86	0.89	0.80	0.78
CTree	0.64	0.65	**0.83**	0.90	**0.91**	0.85	0.91	**0.87**	0.81	**0.91**	0.85	0.80	0.83
LR	**0.79**	0.73	0.82	0.88	0.87	0.81	**0.93**	0.78	0.72	0.90	**0.92**	0.77	0.83
RF	0.73	**0.80**	**0.83**	**0.92**	0.90	**0.88**	0.86	0.85	**0.83**	0.89	0.91	**0.81**	**0.85**

*Bold number denotes the highest accuracy among the four algorithms.

CONCLUSIONS

This paper presents a novel approach to non-intrusively obtain, retrieve, and analyze facial skin temperature data and interpret occupants' thermal preferences using low-cost infrared thermography. The proposed approach leverages interdisciplinary techniques including the thermoregulatory theory, computer vision, and machine learning. Results demonstrate that ears, nose, and cheeks region have a larger skin temperature variation under cold and heat stress. Therefore, features retrieved from these regions are most indicative of thermal comfort. In addition, facial skin temperature data collected from the low-cost infrared thermal camera were used to develop personal comfort models using four machine learning algorithms. The results show that the Random Forest algorithm has the best performance and can achieve an 85% accuracy in thermal comfort prediction, which offers the possibility for synchronous control of indoor environments with minimal interruption of building occupants. The resulting new knowledge from this study has the potential to transition the current building HVAC control from a passive and user-empirical process to an automated, user-centric, and data-driven mechanism that can simultaneously improve occupant satisfaction and well-being in indoor environments.

ACKNOWLEDGMENTS

The authors would like to acknowledge the financial support for this research received from the U.S. National Science Foundation (NSF) CBET 1349921 and CBET 1804321. Any opinions and findings in this paper are those of the authors and do not necessarily represent those of the NSF.

APPENDIX

Table A.1. Statistics of skin temperature features in the three phases

Features	Cooling		Heating		Steady-State	
	$\bar{\mu} \pm SD(\bar{\mu})$ (1)	$\bar{s} \pm SD(\bar{s})$ (2)	$\bar{\mu} \pm SD(\bar{\mu})$ (3)	$\bar{s} \pm SD(\bar{s})$ (4)	$\bar{\mu} \pm SD(\bar{\mu})$ (5)	$\bar{s} \pm SD(\bar{s})$ (6)
maxVal	**34.38±0.84**	**0.31±0.11**	**34.17±0.93**	**0.12±0.04**	**34.52±0.62**	**0.08±0.03**
∇maxVal	-.016±.005	.013±.006	.004±.003	.009±.002	-.003±.003	.006±.003
forehead_avg	**33.55±0.92**	**0.34±0.15**	**33.02±1.50**	**0.19±0.11**	**33.77±0.73**	**0.07±0.02**
forehead_max	34.17±0.86	0.33±0.13	34.01±1.08	0.13±0.05	34.49±0.62	0.09±0.03
forehead_min	30.05±0.72	0.44±0.25	29.58±0.48	0.20±0.17	30.16±0.71	0.10±0.09
∇forehead	-.018±.007	.013±.005	.006±.009	.010±.002	-.002±.002	.006±.003
nose_avg	**32.46±1.61**	**0.60±0.25**	**31.85±0.66**	**0.77±0.34**	**32.38±1.54**	**0.22±0.11**
nose_max	33.33±1.20	0.45±0.17	32.80±0.58	0.46±0.17	33.21±1.07	0.17±0.09
nose_min	30.87±2.51	0.56±0.20	30.29±1.50	0.81±0.33	31.15±2.05	0.20±0.08
∇nose	-.032±.012	.022±.009	.032±.021	.034±.015	-.007±.007	.017±.012
cheek_avg	**32.35±1.84**	**0.35±0.15**	**31.86±1.66**	**0.31±0.12**	**32.70±1.46**	**0.09±0.05**
cheek_max	33.62±1.35	0.28±0.15	33.21±1.16	0.22±0.08	33.73±1.12	0.10±0.04
cheek_min	29.47±2.40	0.53±0.19	29.05±2.18	0.56±0.23	30.32±1.98	0.11±0.05
∇cheek	-.017±.006	.018±.005	.016±.006	.010±.002	-.001±.005	.007±.003
mouth_avg	**33.42±1.04**	**0.32±0.13**	**32.54±1.10**	**0.17±0.05**	**33.30±0.90**	**0.17±0.06**
mouth_max	33.96±0.95	0.28±0.16	33.43±0.81	0.15±0.06	33.88±0.81	0.12±0.04
mouth_min	32.75±1.28	0.42±0.16	31.69±1.39	0.26±0.13	32.66±1.10	0.20±0.08
∇mouth	-.016±.006	.019±.010	.004±.006	.015±.008	.000±.007	.013±.005
ear_avg	**27.01±1.36**	**0.67±0.20**	**26.59±1.47**	**0.71±0.43**	**27.61±1.51**	**0.11±0.05**
ear_max	29.76±1.81	0.62±0.20	29.21±2.02	0.70±0.38	30.35±1.66	0.19±0.08
ear_min	25.30±1.12	0.66±0.25	24.69±1.21	0.60±0.46	25.67±1.39	0.15±0.10
∇ear	-.035±.010	.032±.090	.039±.024	.021±.014	.003±.005	.010±.004
neck_avg	**32.75±0.83**	**0.29±0.18**	**32.35±0.96**	**0.24±0.11**	**32.94±0.92**	**0.12±0.06**
neck_max	33.79±0.61	0.30±0.12	33.55±0.64	0.14±0.05	33.90±0.53	0.07±0.03
neck_min	29.78±1.09	0.40±0.29	29.50±1.11	0.38±0.31	30.33±1.28	0.28±0.21
∇neck	-.014±.009	.018±.009	.011±.008	.010±.001	.000±.005	.011±.004

Note: all numbers are in °C

REFERENCES

Charkoudian, N. (2003, May). Skin blood flow in adult human thermoregulation: how it works, when it does not, and why. In *Mayo Clinic Proceedings* (Vol. 78, pp. 603-612). Elsevier.

Department of Energy (DOE), Heating and Cooling (2017). https://energy.gov/public-

services/homes/heating-cooling.
FLIR Lepton with Radiometry Datasheet (2014). https://www.flir.com/globalassets/imported-assets/document/lepton-engineering-datasheet---with-radiometry.pdf
Jazizadeh, F., Ghahramani, A., Becerik-Gerber, B., Kichkaylo, T., & Orosz, M. (2013). Human-building interaction framework for personalized thermal comfort-driven systems in office buildings. *Journal of Computing in Civil Engineering*, *28*(1), 2-16.
Karmann, C., Schiavon, S., & Arens, E. (2018). Percentage of commercial buildings showing at least 80% occupant satisfied with their thermal comfort.
Kim, J., Zhou, Y., Schiavon, S., Raftery, P., & Brager, G. (2018). Personal comfort models: Predicting individuals' thermal preference using occupant heating and cooling behavior and machine learning. *Building and Environment*, *129*, 96-106.
Li, D., Menassa, C. C., & Karatas, A. (2017a). Energy use behaviors in buildings: Towards an integrated conceptual framework. *Energy Research & Social Science*, *23*, 97-112.
Li, D., Menassa, C. C., & Kamat, V. R. (2017b). Personalized human comfort in indoor building environments under diverse conditioning modes. *Building and Environment*, *126*, 304-317.
Li, D., Menassa, C. C., & Kamat, V. R. (2017c). A personalized HVAC control smartphone application framework for improved human health and well-being. In *Computing in Civil Engineering 2017* (pp. 82-90).
Li, D., Menassa, C. C., & Kamat, V. R. (2018). Non-intrusive interpretation of human thermal comfort through analysis of facial infrared thermography. *Energy and Buildings*, *176*, 246-261.
Viola, P., & Jones, M. (2001). Rapid object detection using a boosted cascade of simple features. In *Computer Vision and Pattern Recognition, 2001. CVPR 2001. Proceedings of the 2001 IEEE Computer Society Conference on* (Vol. 1, pp. I-I). IEEE.